An Integrated Shape-Texture Descriptor for Modeling Whole-Organism Phenotypes in Drug Screening

Jiadong Yu1 and Rahul Singh1,2

¹ Department of Computer Science, University of Iowa, Iowa City, Iowa 52242-1419 ² Center for Discovery and Innovation in Parasitic Diseases, UC San Diego, CA 92093 rahul-singh@uiowa.edu

Abstract. Schistosomiasis is a parasitic disease with global health and socioeconomic impacts. The World Health Organization (WHO) and National Institutes of Health (NIH) list it among diseases for which new treatments are urgently required. Drug discovery for Schistosomiasis typically involves wholeorganism phenotypic screening. In such an approach, the parasites are exposed to different chemical compounds, and systemic phenotypic effects captured via microscopy (video or still images) are analyzed to identify promising molecules. Changes in parasite phenotypes tend to be multidimensional, involving changes in shape, appearance and behavior, and time-varying. In many image representation frameworks, shape and appearance are measured independently and their inter-correlation can be lost. In this paper, we propose an integrated shape-texture descriptor called the skeleton-constrained shortest band (SCSB) that extends the family of shape context descriptors well known in computer vision. We examine how SCSB can be used to measure temporally varying shape and appearance changes occurring as a consequence of chemical action and compare its performance with other members of the shape context family.

Keywords: Shape Context, biological imaging, microscopy, parasitic diseases, whole-organism screening, drug discovery.

1 Introduction

1.1 Background

Schistosomiasis is a parasitic disease with global health and socio-economic impacts. It is estimated that over 200 million people are currently infected and more than 700 million are at risk across 78 countries. Treatment is largely based on the drug praziquantel (PZQ). However, it is primarily effective during the adult stage of the worm life cycle [1] and resistance to the drug has been observed [2]. Thus, the World Health Organization (WHO) and National Institutes of Health (NIH) list schistosomiasis among diseases for which new treatments are urgently required.

Drug discovery for Schistosomiasis (and other helminthic diseases) typically involves whole organism phenotypic screening. In this process, parasite(s) are exposed to different compounds and the resultant multidimensional and systemic phenotypic

changes are recorded and analyzed to determine the efficacy of the compounds and identify putative novel drugs. Starting with the pioneering work in [3], the development of phenotype-analysis methods for this area has attracted significant interest. Within this context, one of the key technical challenges lies in the development of image representation-comparison frameworks that can capture the wide variety of correlated shape-appearance changes exhibited by the parasites causing schistosomiasis.

1.2 Problem formulation

In order to precisely measure complex parasite phenotypes, the representation must be accurate, robust, and invariant to the following characteristics: (1) Euclidean and scale invariance, (2) significant deformations that occur as the parasites move, and (3) a range of imaging conditions. Furthermore, shape and appearance changes are not only two of the most important aspects of parasite phenotypic responses, but they can also be correlated. For example, as the shape of the parasite deforms during motion, its body texture changes in a coupled manner. Consequently, integrated shape-texture descriptors are required since measuring these attributes independently may fail to capture their interrelationship.

The example in Figure 1 illustrates these characteristics. In it, a group of parasites exposed to the antipsychotic drug acepromazine are followed across 10 non-consecutive frames. It is easy to note that the illumination changes over the recording time. More importantly, we can observe that the parasite at the bottom left of the top row underwent significant changes in both shape and texture due to its movements. The reader may also note the temporally evolving systemic degradation suffered by the parasites (bottom row) when compared with the top row, as a result of chemical action.

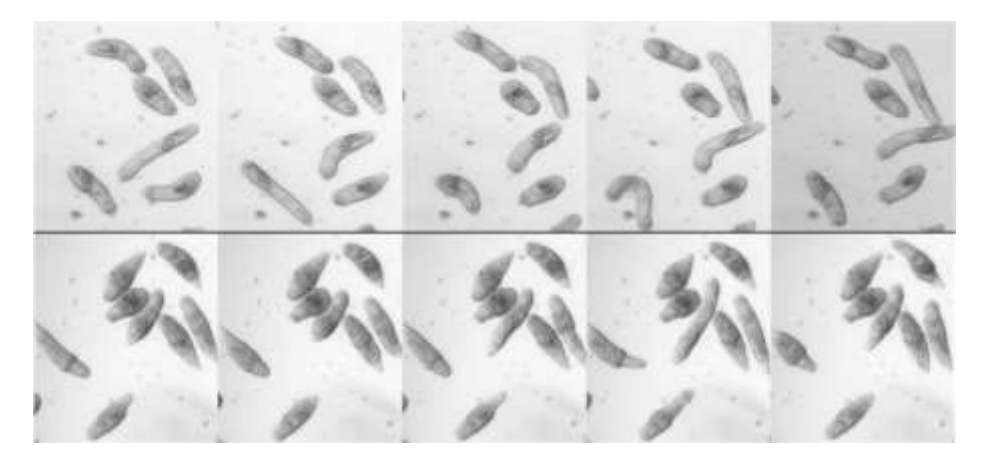


Fig. 1. Depiction of shape and appearance changes over time: top-row due to parasite motion and across top-and bottom row due to chemical action. The top row shows 6 parasites in 5 frames exposed to acepromazine (10 μ M and one day of exposure to the compound). The bottom row shows 5 frames with the parasites also exposed to acepromazine (10 μ M, four days after exposure to the compound).

2 Prior work

The first attempt to describe the complex phenotypes of Schistosomiasis using algorithmic image analysis was made by Singh et al. [3]. In this work the problems of segmentation, appearance encoding, and phenotype classifications were addressed by analyzing parasites exposed to a select set of compounds. The description of the shape and appearance relied on measurements of eccentricity, entropy, and local pixel range. Nevertheless, eccentricity alone is insufficient to fully encompass all of the intricate deformation-driven alterations in the parasite shape. In a significant advancement thereafter, a public webserver called QDREC [4] for automatically determining dose-response characteristics and IC₅₀ values from microscopy images was developed. In QDREC, 71 image-based features were used to describe the shape and appearance. As mentioned above, many these features were calculated independently for shape-appearance changes that are coupled and any interrelationships were, at best, reflected implicitly in QDREC. Method development reported by us in this paper is motivated by the shape-context family of representations. The progenitor of this family of methods, the shape context (SC) representation [5], is known to be a robust shape descriptor that is invariant to translation, rotation, and scale. Its generalization, called the inner distance shape context (IDSC), and a combined descriptor using IDSC and intensity gradient directions called the shortest path texture context (SPTC) were proposed later [6]. However, we have found (and demonstrate in this paper) that IDSC can be sensitive to inconsequential shape variations. Furthermore, intensity gradient directions may be too simplistic to describe complex texture changes.

3 Methods

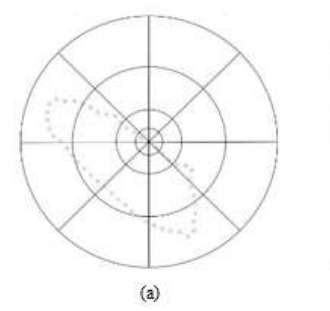
3.1 Integrated Representation of parasite morphology and appearance.

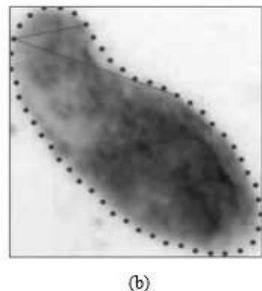
In this section, we start by summarizing the shape context (SC) representation. Given the contours of a parasite $P|P \in \mathbb{R}^2$, the shape context descriptor SC(P) is defined as the relative distribution of each of the contour points of P to the other contour points. That is, for the contour $P = \{c_1, ..., c_n\}$, SC(P)= $\{d_1, d_2, ..., d_n\}$, where d_m is a logpolar histogram capturing the distribution of the contour points $\{c_j \neq c_m\}$ relative to c_m as defined in Eq. (1), where k indexes the bins of the histogram (See Figure 2a).

$$d_m(k) = \#\{(c_j - c_m) \in bin(k), m \neq j\}$$
 (1)

Each histogram d_m can be rotated and positioned based on the tangent line at c_m to obtain rotation invariance. SC is also invariant to Euclidean transformations and is known to be highly noise tolerant. Scale-invariance can be obtained if the radius of the log-polar histogram is calculated using the mean distance between all the points pairs.

In the IDSC, the geodesic distance *i.e.*, the shortest path between a pair of points that is completely contained inside the shape is used to construct the log-polar histogram (Figure 2b). Due to its use of inter-point geodesics, IDSC is invariant to shape articulations. The reader is referred to the original SC and IDSC papers for a detailed technical explanation underlying the characteristics of SC and IDSC methods. However, the geodesic distance uses other points as bridge points if the Euclidean distance between a pair of points doesn't entirely lie within the shape, and as we have found, it is particularly sensitive to small changes on the contour under these conditions.





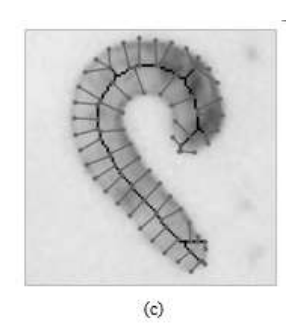


Fig. 2. A figure caption is always placed below the illustration. Short captions are centered, while long ones are justified. The macro button chooses the correct format automatically.

Such sensitivity is of course highly undesirable, since in such cases, the geodesic distance may fluctuate unpredictably for small local changes in the contour. As an alternative we propose a descriptor which constrains the geodesic distances between an arbitrary pair of contour points to pass through the shape skeleton (Figure 2c). The incorporation of the shape skeleton leads to more robust descriptor that is also sensitive to shape articulations when compared to SC and IDSC.

We define the skeleton-constrained inner distance (SCID) for object O with contour P and skeleton $S = \{s_1, ..., s_t\}$ as follows:

$$\alpha(c_i, c_i; 0) = \alpha(c_i, s_i; 0) + \alpha(s_i, s_i; S) + \alpha(s_i, c_i; 0)$$
(2)

$$\alpha(c_i, s_i; 0) = \min\{\alpha(c_i, s_i; 0), c_i \in P \text{ and } \forall s_i \in S\}$$
(3)

In Eq. (2) and (3), $\alpha(c_i, c_j; O)$ is the skeleton-constraint inner distance from $c_i \in P$ to $c_j \in P$, $\alpha(c_i, s_i; O)$ is the shortest (in the least square) sense path from the contour point c_i to the $s_i \in S$ which contained inside the object O, $\alpha(s_j, c_j; O)$ is the shortest (in the least square) sense path between $s_j \in S$ and $c_j \in P$, and $\alpha(s_i, s_j; S)$ is the path from s_i to s_j along the skeleton S. Typically, the skeleton is computed using the media axis transformation and can be sensitive to contour variations leading to unnecessary branching of the skeleton. To improve the robustness, a pruning step is applied to the skeleton. Specifically, the skeleton S is first divided into the main branch S_a and side branches S_i such that:

$$S = S_a \cup \{ \bigcup_i S_i \} \text{ and } S_a \cap S_i = \emptyset, \forall i$$
(4)

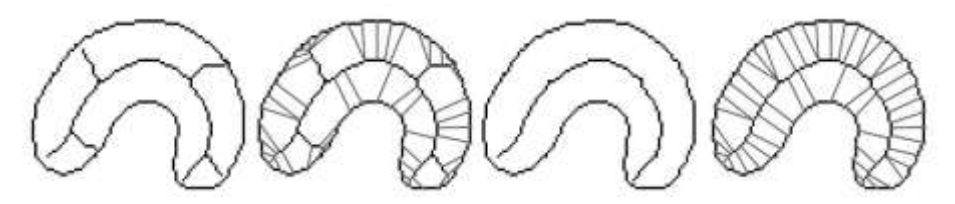


Fig. 3. Skeleton and their skeleton-constrained shortest paths before and after the pruning step. The left two images represent the unpruned version, and the right two images represent the pruned version with only the main branch left.

Subsequently, a proportion of S_i can be pruned based on its characteristics (Figure 3). The pruning is done as the following: (1) The main branch and side branches are identified by measuring the distance along the skeleton between all its endpoints, (2) side branches are ordered by their distance, and (3) the shortest side branches are pruned based on a pruning ratio which can either be user-specified or determined automatically.

To explain our approach to the joint modeling of shape and texture, we begin by noting that in the SPTC by the shape information captured by the IDSC is supplemented by measuring the distributions of (weighted) relative orientation through the shortest paths. The relative orientation is obtained by measuring the angles between intensity gradient directions and shortest path direction, and the weight is gradient magnitudes. The SPTC is a 3-D histogram where the inner-distance and the innerangle used as the first two dimensions are the same as IDSC. The third dimension is binned normalized histogram of weighted relative orientation.

Our approach combines shape and appearance through similarly but uses a different texture descriptor called dominant rotated local binary pattern (DRLBP) [7]. DRLBP is a rotation invariant texture descriptor that builds on top of the local binary pattern (LBP), where the central pixel of a local circular region is compared with its neighbors.

$$LBP_{R,B} = \sum_{b=0}^{B-1} s(p_b - p_c) \cdot 2^b$$
 (5)

In Eq. (5), p_c and p_b denote the gray level intensity of the central pixel and its neighbors, R is the radius of the circular neighborhood, B the number of neighbors, and s is an indicator function where its value is 0 if the neighbor pixel is less than the central pixel, 1 otherwise. A dominant direction is then defined (Eq. (6)), which can be used to rotate the LBP and thereby achieve rotational invariance (Eq. (7)).

$$DIR = \arg\max_{b \in (0,1,\dots,B-1)} |p_b - p_c|$$
 (6)

$$DRLBP_{R,B} = \sum_{b=0}^{B-1} s(p_b - p_c) \cdot 2^{mod(b-DIR,B)}$$
 (7)

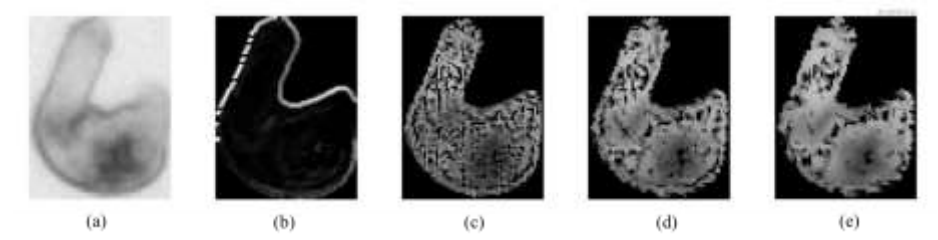


Fig. 4. Appearance and texture of a parasite using relative orientation and DRLBP. (a) Original parasite, (b) Weighted relative orientation. (c)(d)(e) Weighted Rotated Local Binary Pattern (WRLBP) with radii 1, 2, 3, respectively.

DRLBP is invariant to illumination due to the indicator function. It is also a more flexible and informative texture descriptor as a broader range of neighborhood pixels can be considered with the radius parameter (Figure 4). To distinguish darker parasites from lighter ones, even when they are similarly textured, we can weigh the RLBP as the following:

$$WRLBP_{R,B} = DRLBP_{R,B} \cdot \frac{p_c}{2^B} \tag{8}$$

Finally, to obtain the integrated shape-appearance description of an object O with contour P, which we shall call the skeleton-constrained shortest band (SCSB), $\alpha(c_m, c_j; O)$ is the shortest path between the contour point c_m and c_j of P as defined above. The new k^{th} bins of the 3D-histogram can be formulated as the following:

$$d_m(k) = \#\{p_i \in bin(k), p_i \in \alpha(c_m, c_i; WRLBP_{RR}(O))\}$$

$$\tag{9}$$

where $WRLBP_{R,B}(O)$ is the appearance of object O and p_i are the pixels along the SCID inside $WRLBP_{R,B}(O)$.

To match two objects with their histograms, we must find the point correspondences and compute the dissimilarity score between them. The dissimilarity between the contour points from one object to another is calculated as the χ^2 distance between their corresponding histograms:

$$cost(c_i^P, c_j^Q) = \chi^2(d_i^P, d_j^Q) = \frac{1}{2} \sum_{k=1}^K \frac{[d_i^P(k) - d_j^Q(k)]^2}{d_i^P(k) + d_j^Q(k) + \varepsilon}$$
(10)

In Eq. (10), d_i^P represents the histogram computed at point c_i of an object with contour P and $cost(c_i^P, c_j^Q)$ represents the dissimilarity in terms of χ^2 distance between histograms d_i^P and d_i^Q .

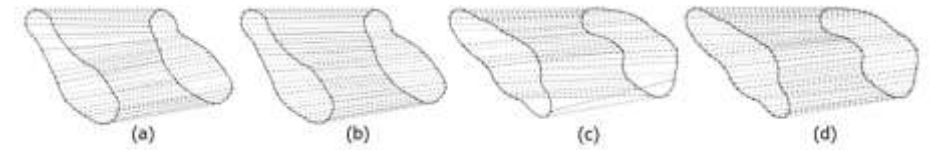


Fig. 5. Matching of two pairs of parasites using the Hungarian methods, DP method with a threshold parameter 0.3, and circular matching: (a), (c) Matching using DP method with a threshold parameter 0.3. (b), (d) Matching using circular matching.

Given a set of $cost(c_i^P, c_i^Q)$ of all the points between two objects, the final dissimilarity score and correspondences can be computed by obtaining correspondences between pairs of contour points. Such a correspondence can be obtained either by using the Hungarian algorithm with additional "dummy" points used by Belongie et al. [5] or by dynamic programming (DP), as proposed by Ling et al [6]. However, both approaches are problematic. The Hungarian algorithm computes the optimal cost between two objects but doesn't consider the connectivity constraints between contour points leading to non-monotonic matching of point pairs. The "dummy" points introduce a constant cost and can be treated as a threshold parameter to filter out the pairs of points with high-cost scores. However, this doesn't consider the non-monotonic matching with low-cost scores. In our case, this parameter is hard to choose as large deformation can result in a higher cost score while small deformation can result in a lower cost score and the final dissimilarity score could be inconsistent due to the choice of the threshold parameter. See Figure 5a and 5c, the correspondences for the same threshold 0.3 works very differently when large and medium deformation appears. Therefore, we use a similar approach to the DP method but enforce all matching without the threshold parameter as this is better at presenting dissimilarity score involving large deformation, and we call this circular matching (CM) (Figure 5b and 5d).

Table 1. Statistical summary of the dataset

	Dataset
Total parasites	175
The size of parasites	2314 - 6668
Perimeter of parasites	166 - 390
Proportion of the bbox filled	19% - 79%
Grayscale mean intensity	108 - 196
Exposure time in days	1, 2, 3, 4, 7
Concentration in μM	0*, 0.01, 0.1, 1, 10
Compounds	Acepromazine, Alimemazine, Amitriptyline, Chlorophenothiazine, Clomipramine, Cyclobenzaprine, Desipramine, Hycanthone, Imipramine, K777, Methiothepin Mesylate, Mevastatin, Niclosamide, Pravastatin, Praziquantel (PZQ), Promazine, Promethazine, Rosuvastatin, Simvastatin, Triflupromazine, Control*

4 Experiments

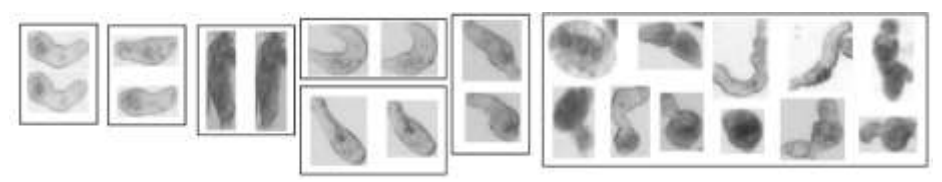


Fig. 6. The comprehensive datasets. Left are examples from the 50 paired parasites. Right are examples from the 75 unique parasites.

The proposed methods are evaluated with a comprehensive chemical-phenotype dataset that was reported in [8]. It contains 50 paired parasites from consecutive frames of the same video include small, medium and large deformations, and 75 parasites with unique phenotypes (Figure 6). A summary of the dataset is provided in Table 1. Now we describe the parameter used through all the experiments. We use n to denote the number of sample points on the outer contour of the shapes. As n gets large, is the contour representation becomes more accurate but less efficient. For the size of histograms, n_r , n_t , and n_i are used for the number of bins for log-distance on the radius, the number of bins for the angles, and the number of bins for the intensity levels, respectively. For the pruning fraction used to prune branches of the skeleton, f is used. In our work, a typical setting for these parameters was $n_r = 5$, $n_t = 12$, $n_i = 16$, f = 0.25 and are used through all the experiments in this paper.

4.1 Shape Retrieval in terms of deformation

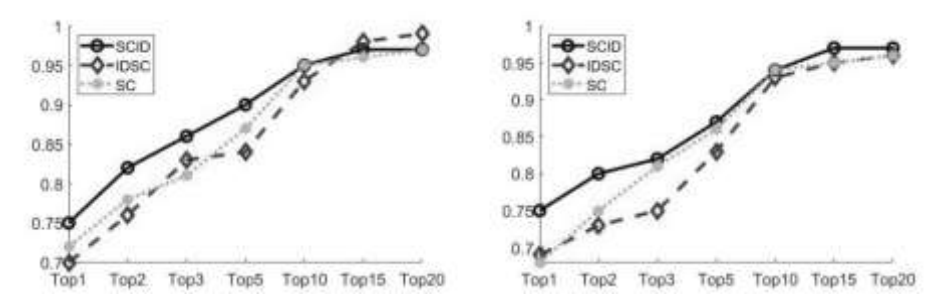


Fig. 7. Two case studies on shape retrieval in terms of deformation. (a) Case study one with 100 parasites. (b) Case study two with 175 parasites.

Although SCID does not explicitly factor-in deformation, it is relatively robust for deformable shape retrieval when compared to SC and IDSC. The 50 pairs of parasites from consecutive frames show a variety of cases when small, medium, and large deformations are observed to occur in the Dataset (see Figure 6). We designed two case studies to compare SCID, IDSC, and SC. Both the case studies go through the same step. For each of the 100 parasites (50 pairs), if the desired shape (the other parasite in the pair) appears in the top K retrievals, it is considered a hit (the parameter K is var-

ied as part of the study). A percentage can be calculated based on the number of hits for all the 100 parasites.

The first case study query uses only the 50 pairs of the parasites (total of 100), while the second case study query uses all the 175 parasites in the Dataset. See Figure 7. SCID shows better shape retrieval compared to IDSC and SC. Both case studies lead to similar conclusions, *i.e.*, SCID is better at shape retrieval when deformation are presents, especially when $K \le 10$ corresponding to the requirement of high precision in the retrievals.

4.2 Robustness and Sensitivity

In this section, we compare the sensitivity of SCID and IDSC. We have noted that IDSC may be sensitive to small changes on the contour while SCID is not. An example is shown in Figure 8.

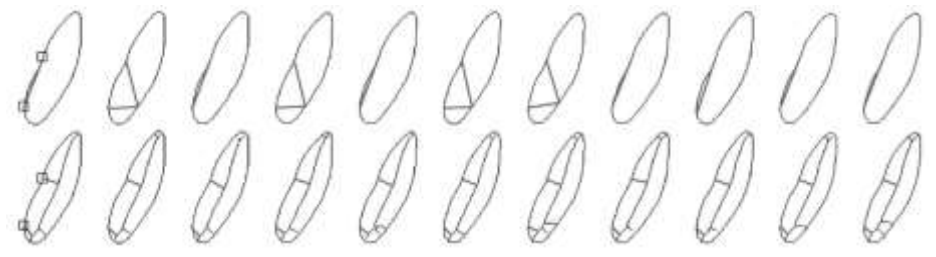


Fig. 8. Fluctuations in the IDSC (top row, showing the shortest paths) and SCID between the same two points of the same parasite taken from 11 consecutive frames.

We can observe that the shape changes between these 11 consecutive frames are small. However, the shortest path inner distance fluctuates between the two points across the frames resulting in inconsistent dissimilarity scores. In Figure 9, these dissimilarity scores are shown for both IDSC and SCID. Clearly, SCID is more robust and less sensitive than IDSC for this example with small contour variations.

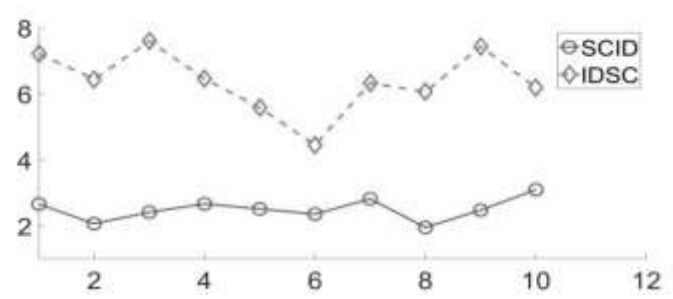


Fig. 9. Dissimilarity scores between 11 parasites in successive frames using both SCID and IDSC. Unlike the SCID curve, the IDSC curve shows large fluctuation even when parasite shapes show small changes.

For significant deformations, the fluctuations in the geodesic distance used in IDSC are greater as compared to the SCID. To demonstrate this, consider the following five parasites across 11 consecutive frames (Figure 10).

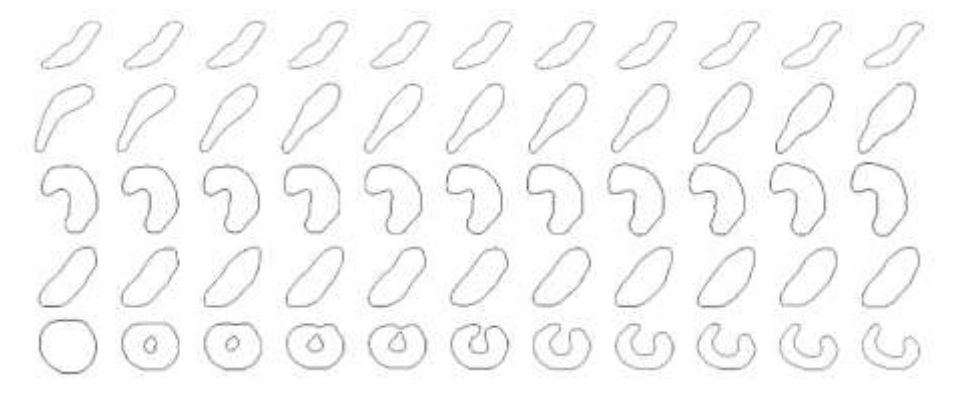


Fig. 10. 5 parasite contours across 11 consecutive frames exhibiting significant shape deformations.

Instead of determining the shortest path using IDSC and SCID between two specific points of these parasites as in the previous experiment, we compute a more holistic statistic obtained by determining the variances of the shortest path distances between all paired points across the 11 frames for these two methods. For each of the five parasites, a pair of boxplots is used to present a side-by-side comparison of the variances in Figure 11.

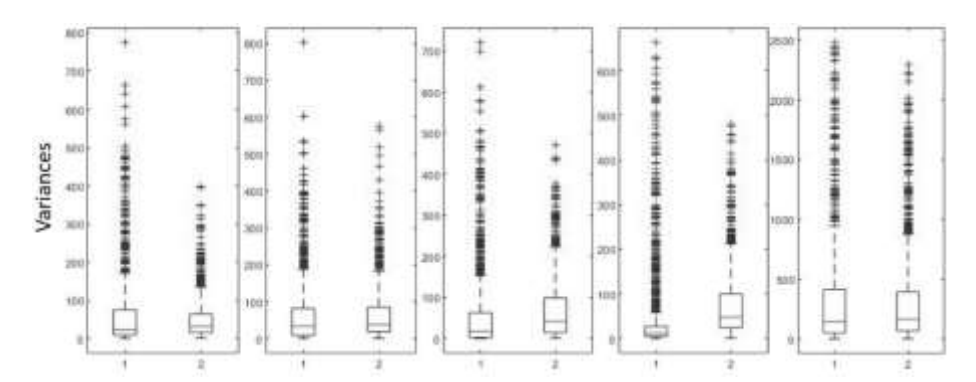
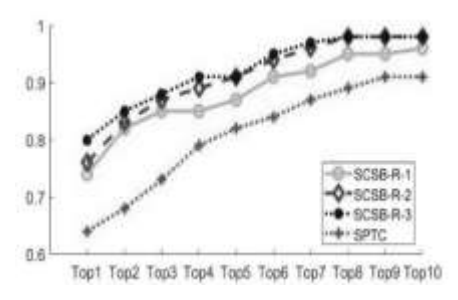


Fig. 11. The boxplots from left to right correspond to the parasites (and their deformations) shown from top to bottom in Figure 10. The label 1 in each boxplot denotes the variance of IDSC while the label 2 denotes the variances of SCID.

The reader may note that both IDSC and SCID show large variances for large shape deformations. However, the variances in SCID measurements are always less than the corresponding variances in the IDSC measurements. These two experiments demonstrate the robustness of the SCID representation.

4.3 Phenotype Retrieval



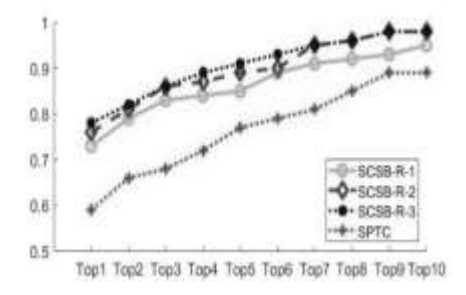


Fig. 12. Two case studies on shape retrieval in terms of deformation: (left) Case study with 100 parasites. (right) Case study with the set of 175 parasites.

In the previous section, we showed how SCID compared with SC and IDSC. Using the same experimental settings we compare the SPTC with the SCSB (using radii of 1, 2, and 3). In Figure 12, the retrieval performances are shown for the top-K hits ($K \le 10$). SCSB is found to consistently perform better than SPTC across all the values of K with the best results obtained with the radius value of 3.

5 Conclusion

This paper describes a novel shape-texture descriptor based on a new inner-distance formulation called skeleton-constraint inner distance and compares it to prior shape context formulations. Preliminary results on phenotypic screening data underline the robustness and promise of the proposed approach for shape and appearance matching.

Acknowledgements. The authors thank Conor R. Caffrey for the screening data reported in [8]. This work was funded by NSF (IIS 1817239) and NIH (AI146719).

References

- Vale, N., Gouveia, M.J., Rinaldi, G., Brindley, P.J., Gärtner, F., Correia Da Costa, J.M.: Praziquantel for Schistosomiasis: Single-Drug Metabolism Revisited, Mode of Action, and Resistance. *Antimicrobial Agents and Chemotherapy* 61, e02582-16 (2017). https://doi.org/10.1128/AAC.02582-16
- Fallon, P.G.: Schistosome resistance to praziquantel. *Drug Resistance Updates*. 1, 236–241 (1998). https://doi.org/10.1016/S1368-7646(98)80004-6
- 3. Singh, R., Pittas, M., Heskia, I., Xu, F., McKerrow, J., Caffrey, C.R.: Automated image-based phenotypic screening for high-throughput drug discovery. In: 22nd *IEEE International Symposium on Computer-Based Medical Systems*. pp. 1–8. IEEE, Albuquerque, NM, USA (2009)

- Asarnow, D., Rojo-Arreola, L., Suzuki, B.M., Caffrey, C.R., Singh, R.: The QDREC web server: determining dose–response characteristics of complex macroparasites in phenotypic drug screens. *Bioinformatics*. 31, 1515–1518 (2015). https://doi.org/10.1093/bioinformatics/btu831
- Belongie, S., Malik, J., Puzicha, J.: Shape matching and object recognition using shape contexts. *IEEE Transactions on Pattern Analysis and Machine Intelligence* 24, 509–522 (2002). https://doi.org/10.1109/34.993558
- Ling, H., Jacobs, D.W.: Shape Classification Using the Inner-Distance. *IEEE Transactions on Pattern Analysis and Machine Intelligence* 29, 286–299 (2007). https://doi.org/10.1109/TPAMI.2007.41
- Mehta, R., Egiazarian, K.: Dominant Rotated Local Binary Patterns (DRLBP) for texture classification. *Pattern Recognition Letters* 71, 16–22 (2016). https://doi.org/10.1016/j.patrec.2015.11.019
- 8. Lee, H., Moody-Davis, A., Saha, U., Suzuki, B.M., Asarnow, D., Chen, S., Arkin, M., Caffrey, C.R., Singh, R.: Quantification and clustering of phenotypic screening data using time-series analysis for chemotherapy of schistosomiasis. *BMC Genomics*. 13, S4 (2012). https://doi.org/10.1186/1471-2164-13-S1-S4